Testing models of accreting stars in massive binaries on ζ Ophiuchi

M. RENZO[1,2] AND Y. GÖTBERG[3]

[1]*Department of Physics, Columbia University, New York, NY 10027, USA*
[2]*Center for Computational Astrophysics, Flatiron Institute, New York, NY 10010, USA*
[3]*The Observatories of the Carnegie Institution for Science, 813 Santa Barbara Street, Pasadena, CA 91101, USA*

ABSTRACT

Binarity dominates the evolution of massive stars, and the nearest O-type star to Earth, ζ Ophiuchi, has long been proposed to be a product of binary evolution. Despite this, most stellar models have tried unsuccessfully to reproduce its observable properties relying on single-star rotating models. ■ [Here we do better] ■

Keywords: stars: individual: ζ Ophiuchi – stars: massive – stars: binaries

1. INTRODUCTION

The overwhelming majority of massive stars is born in multiple systems (e.g., Mason et al. 2009; Almeida et al. 2017), and a large fraction will exchange mass or merge with a companion in their lifetime (e.g., Sana et al. 2012). The most common type of interaction is a post-main-sequence stable mass transfer (case B) through Roche Lobe overflow (RLOF, Kippenhahn & Weigert 1967, ■ [pop synth. ref.?] ■. Many studies (e.g. Götberg et al. 2017, 2018; Laplace et al. 2020, 2021) have focused on the dramatic impact of these interactions on the donor star, often treating the closest binary companion as a point mass. ■ [more refs, other groups] ■

However, binary interactions have a crucial impact on the secondary star too. Because of mass transfer, these are expected to accrete mass and rejuvenate because of the accompanying growth of the convective core (e.g., Neo et al. 1977; Schneider et al. 2016), spin up to critical rotation (e.g., Packet 1981; Cantiello et al. 2007), and possibly be polluted by CNO-processed material from the inner core of the donor star (e.g., Blaauw 1993).

Understanding the evolution of accretors in massive binaries has wider and crucial implications for stellar populations, electromagnetic transient observations, and gravitational-wave progenitors. Binary products, and accretors in particular, can impact cluster populations and their age estimates and main sequence morphology (e.g., Pols & Marinus 1994; Wang et al. 2020). Moreover, the majority of massive binaries will be disrupted by the first supernova ejecting the companion ("binary SN scenario", Blaauw 1961; De Donder et al. 1997; Eldridge et al. 2011; Renzo et al. 2019; Evans et al. 2020). Therefore, populations of field massive stars contain presently single O-type stars that accreted mass earlier on. The majority of these will be too slow to stand out in astrometric surveys (e.g., Eldridge et al. 2011; Renzo et al. 2019). Assuming a constant star formation history, Renzo et al. (2019) estimated that $10.1^{+4.6}_{-8.6}\%$ of O-type stars might be accretors released after a SN – where the errors span a range of parameter variations.

From the transients perspective, accretors stars are also important: Zapartas et al. (2019) showed that $14^{+4}_{-11}\%$ of hydrogen-rich (type II) SNe might come from these progenitors after being ejected from a binary. The fact that they accreted mass before exploding can influence their helium (He) core mass and thus the explosion properties and the inferred progenitors (Zapartas et al. 2021).

Finally, the majority of isolated binary evolutionary scenarios for gravitational-wave progenitors go through a common-envelope phase initiated by the originally less massive accretor after the formation of the first compact object (e.g., Belczynski et al. 2016; Tauris et al. 2017; Broekgaarden et al. 2021). Therefore, it is possible that accretion of mass before the formation of the first compact object could modify the internal structure of the star that will initiate the common-envelope phase (e.g. Law-Smith et al. 2020; Klencki et al. 2021).

Despite their importance, accretor stars in binaries have so far received much less attention than the donor stars, with the pioneering work of Hellings (1983, 1984) and Braun & Langer (1995) as notable exceptions. Large grids of accretor models are missing, and only sparse models exist (e.g., Cantiello et al. 2007)■ [more refs.] ■. This is because of the complexity of these models, where one needs to follow in detail the *coupled* evolution of two rotating stars exchanging mass.

Moreover, the admittedly large number of free parameters involved in the modeling of each individual star and their interactions makes robust predictions challenging to obtain. Here, we will argue that the nearest O-type star to Earth, ζ Ophiuchi[1] (ζ Oph) provides a unique opportunity to constrain these models.

ζ Oph has a distance from Earth of $107 \pm 4\,\mathrm{pc}$ (Neuhäuser et al. 2020, and references therein), and a spectral type O9.5IVnn (Sota et al. 2014). It occasionally shows emission lines (Walker et al. 1979; Vink et al. 2009), making it an Oe star. It was originally identified as a runaway because of its large proper motion by Blaauw (1952). Unfortunately, the *Gaia* data for this object are not of sufficient quality[2] to improve previous astrometric results, but estimates of the peculiar velocity range in $30 - 50\,\mathrm{km\ s^{-1}}$ (e.g., Zehe et al. 2018; Neuhäuser et al. 2020). The large velocity with respect the surrounding interstellar material is also confirmed by the presence of a prominent bow-shock (e.g., Bodensteiner et al. 2018).

Because of its young apparent age, extremely fast rotation ($v \sin(i) \gtrsim 400\,\mathrm{km\ s^{-1}}$, e.g., Zehe et al. 2018), and nitrogen (N) and He rich surface (e.g., Herrero et al. 1992; Blaauw 1993; Villamariz & Herrero 2005; Marcolino et al. 2009), ζ Oph is a prime candidate for the binary SN scenario (Blaauw 1993). Many studies have suggested ζ Oph might have accreted mass from a companion before acquiring its large velocity, both from spectroscopic and kinematic considerations (e.g., Blaauw 1993; Hoogerwerf et al. 2000, 2001; Tetzlaff et al. 2010; Neuhäuser et al. 2020) and using stellar modeling arguments (e.g., van Rensbergen et al. 1996). Recently, Neuhäuser et al. (2020) suggested that a supernova in Upper-Centaurus-Lupus produced the pulsar PSR B1706-16, ejected ζ Oph, and also injected the short-lived radioactive isotope ^{60}Fe on Earth $1.78 \pm 0.21\,\mathrm{Myr}$ ago. This argues strongly for a successful supernova explosion accompanied by a large $\sim 250\,\mathrm{km\ s^{-1}}$ natal kick, which in most cases would be sufficient to disrupt the binary.

Although the nature of ζ Oph as a binary product is well established, its observed large surface rotation rate has lead previous attempts to rely on rotational mixing to explain the surface composition (e.g., Maeder & Meynet 2000). Even the binary models of van Rensbergen et al. (1996) assumed spin-up due to mass accretion to drive rotational mixing from the interior of the accreting star (see also Cantiello et al. 2007). However,

Villamariz & Herrero (2005) were unable to find good fit for the stellar spectra using the rotating models from Meynet & Maeder (2000).

This may not be surprising: rotational mixing has lower efficiency for metal-rich and relatively low mass stars because of the increased importance of mean molecular weight gradients and longer thermal timescales compared to more massive stars (e.g., Yoon et al. 2006; Perna et al. 2014). The parent association has a metallicity $Z = 0.01 \simeq Z_{\odot}$ (based on asteroseismology from Murphy et al. 2021), and mass estimates for ζ Oph range from $13 - 25\,M_{\odot}$, at the lower end of the range where efficient mixing might bring He and CNO-processed material to the surface (chemically homogeneous evolution).

■ **[maybe paragraph below goes in discussion]** ■ On top of the surface abundances, its extreme rotation rate, and the peculiar space velocity, ζ Oph poses a number of other puzzles: its wind mass-loss rate is about two orders of magnitude lower than theoretical predictions (weak wind problem, Marcolino et al. 2009), the star exhibits spectral variability with occasional appearance of Hα in emission (e.g., Walker et al. 1979), and is potentially magnetic ■ **[true?ref?]** ■.

Given the challenges in explaining the surface composition of ζ Oph with rotational mixing from the stellar interior and the strong evidence for its past as a member of a binary system, this star offers a unique opportunity to constrain the evolution of accreting stars in massive binary systems.

Here, we present self-consistent binary evolution models for ζ Oph computing simultaneously the coupled evolution of *both* donor and accretor star and their orbit. ■ **[fix order description]** ■ After presenting our calculations in Sec. 2, we show our best model which reproduces the majority of the salient features of this star in Sec. 3. In this model, the surface abundances of ζ Oph are explained by pollution from the former companion, rather than upward mixing from the interior of ζ Oph itself. We discuss the sensitivity of our results to the admittedly many free parameters required for this kind of computations in Sec. 4. Finally, we conclude in Sec. 6.

2. MESA MODELING OF MASSIVE BINARIES

Modeling the evolution of massive binaries ($M_1 \gtrsim 20\,M_{\odot} \geq M_2$) is challenging because of the intricate role of several notoriously difficult stellar physics ingredients (differential rotation, mixing, high mass-loss rates, accretion, etc.). Here we follow self-consistently the coupled evolution of two massive stars in a binary system using MESA (version 15140). Our choice of in-

---

[1] also known as HD 149 757.

[2] The renormalized unit weighted error (RUWE) of this star in Gaia EDR3 is 4.48.

put parameters and our numerical results are available at ■ [link] ■. We discuss here only the main relevant physical parameters, and Appendix A gives more details on our choice of input physics.

We adopt the Ledoux criterion to determine convective stability and a mixing length parameter of 1.5. We include semiconvection and thermohaline mixing following Langer et al. (1983) and Kippenhahn et al. (1980), respectively, each with efficiency 1.0. We use the exponential core overshooting from Herwig (2000) with free parameters $(f, f_0) = (4.25 \times 10^{-2}, 10^{-3})$ (Claret & Torres 2017) which broadly reproduce the width of the main sequence from Brott et al. (2011). We also use the local implicit enhancement of the convective flux in superadiabatic regions (`MLT--`) introduced in `MESA` 15140.

We treat rotation in the "shellular" approximation and initialize it assuming tidal synchronization at the beginning of the evolution. For our fiducial period choice ($P = 100$ days), this effectively means both the stars in our binary are initially slow rotators. Our models include in a diffusive approximation the effect of Eddington-Sweet circulations (Sweet 1950), which dominates the chemical mixing due to rotation. We also include the secular and dynamical shear instabilities, and the Goldreich-Schubert-Fricke instability as in Götberg et al. (2017, 2018); Laplace et al. (2020, 2021). We assume a Spruit-Tayler dynamo for the transport of angular momentum (Spruit 2002), and chose the same free parameters as Heger et al. (2000). This also includes the rotational enhancement of wind mass loss as in Langer (1998).

We treat wind mass loss with the Vink et al. (2000, 2001) hot wind, and de Jager et al. (1988) with a scaling factor of 1. This effectively means our wind mass loss rate post-mass transfer is overestimated by almost a factor of 100 (weak wind problem, see Marcolino et al. 2009).

Both stars are evolved simultaneously on the same timesteps until after the donor detaches from its Roche lobe. We follow Kolb & Ritter (1990) to calculate the mass transfer rate from optically thick layers of the donor star during Roche lobe overflow (RLOF). Moreover, we assume that the transfered layers reach the accretor with the accretor's specific surface angular momentum and entropy, but the chemical composition is determined by the inner evolution of the donor star. Mass transfer is conservative until the accretor reaches critical rotation, after which rotationally enhanced mass loss governs the accretion efficiency.

To define RLOF detachment, we take advantage of the fact that we focus here on case B interactions among massive stars. After losing its envelope, massive donors
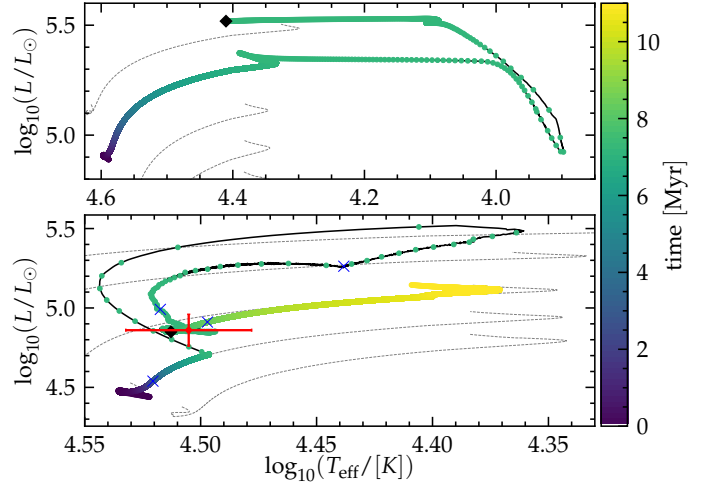

Figure 1. HRD for the donor star (top) and accretor star (bottom) of the progenitor binary of ζ Oph. Each point is separated by 50 years of evolution. The colors represent the stellar age, the red datapoint shows the position of ζ Oph according to Villamariz & Herrero (2005), thin blue crosses mark the position of the profiles shown in Fig. 3 and the black diamonds mark the position at the end of the binary run. We continue the accretor evolution as a single star from there until core H depletion, hence the bottom panel shows a longer time. We emphasize the different scales on the two panels. The thin gray dashed line show the main sequence evolution of non-rotating single stars of 15, 17, 25, and 30 $M_\odot$ at $Z = 0.01$ for comparison.

are not expected to expand to hundreds of $R_\odot$ during He shell burning at the metallicity we consider (e.g., Laplace et al. 2020). Thus, we define RLOF detachment as the moment after the onset of RLOF when the donor has a surface He mass fraction larger than 0.35 (indicating that a significant amount of envelope has been lost or transferred), a radius smaller than its terminal-age main sequence (TAMS, defined as when the central mass fraction of H drops below 10^4) radius, and no mass is being transferred anymore. At this point in time, we save a model for the accreting star, and continue its evolution as a single star until TAMS with the same setup.

■ [describe parameter variations in this sec.] ■

3. MASSIVE BINARY EVOLUTION NATURALLY EXPLAINS ζ OPHIUCHI'S PROPERTIES

We describe here the evolution of a binary system where the accretor star can broadly reproduce all the observed features of ζ Oph. We assume initial masses $M_1 = 25 \, M_\odot$, $M_2 = 17 \, M_\odot$ on a period of 100 days at $Z = 0.01$.

Fig. 1 shows the Hertzsprung-Russell diagrams (HRD) of both stars. After 7.24 Myr, the donor star (top panel)

evolves off the main sequence and ~ 8400 years later, when the donor's effective temperature reaches about $T_{\mathrm{eff}} \simeq 10^4$ K, mass transfer starts. This results in a stable case B RLOF. We refer to Götberg et al. (2017); Laplace et al. (2021); Blagorodnova et al. (2021) and references therein for a detailed description of the evolution of massive donor stars in binaries. Although our models here are more massive, the qualitative behavior of the donor star is similar.

At the onset of RLOF, the accretor star (bottom panel of Fig. 1) is still on the main sequence with $T_{\mathrm{eff}} \simeq 10^{4.5}$ K. Because of accretion, it quickly becomes over-luminous ($L \simeq 10^{5.4} L_\odot$), and its radius increases dramatically from $\sim 7.5 R_\odot$ to $\sim 35 R_\odot$. Once the accretor reaches critical rotation (roughly at the lowest T_{eff} in the bottom panel of Fig. 1), the star begins contracting and its T_{eff} increases. At $T_{\mathrm{eff}} \simeq 4.43$ K the material transferred from the companion star becomes progressively more He-rich, causing a "v-shaped" feature in the evolutionary track. This indicates that the outer layers of the donor's core are uncovered by mass transfer, after the convective core recession in mass during the main sequence. On top of modifying the morphology of the evolutionary track, this late mass transfer puts material at high mean molecular weight μ on top of the primordial envelope of the accretor. This also starts vigorous thermohaline mixing in the accreting star, which, together with rotational mixing, progressively dilutes the surface He and N mass fractions and causes noisy features on the HR diagram (e.g., Cantiello et al. 2007). Sec. 3.1 describes in more detail the mixing processes inside the accretor, we emphasize here that the algorithmic choices made to model mixing might impact the morphology of the accretor's evolutionary track during RLOF.

We evolve the binary system until the black diamonds in Fig. 1, which occurs well after the donor detaches from the Roche Lobe. At this point, the accretor is a H-rich fast-rotating star of $\sim 20.1 M_\odot$. Available mass estimates for the presently single ζ Oph are highly uncertain, but most include $20 M_\odot$ (e.g., Hoogerwerf et al. 2001; Villamariz & Herrero 2005; Neuhäuser et al. 2020). The accretor's post-RLOF orbital velocity is $v_2 \simeq 40$ km s^{-1}, which is expected to decrease a bit further due to wind-driven widening of the binary, but is in good agreement with the presently observed runaway velocity of ζ Oph.

Accounting for both wind mass loss and the amount of mass transferred, at the end of RLOF the donor becomes a He star of $\sim 9.4 M_\odot$, likely to contract further and appear as a Wolf-Rayet star. It's surface H mass fraction is $\lesssim 0.2$ and most of the H is likely to be removed by further wind mass loss (e.g., Götberg et al. 2017). ■ [Ylva: want to expand?] ■. ■ [maybe more next paragraph to discussion?] ■ For our assumed scenario to work, such donor needs to successfully explode in a SN, breaking the binary system and making a neutron star remnant. While the post-RLOF donor mass we obtain is rather high, recent studies suggest higher "explodability" of donor stars in binary systems (e.g., Schneider et al. 2021; Laplace et al. 2021; ?). Furthermore, we emphasize that neither the initial donor mass nor the initial period are observable, and thus there is room to chose different values to obtain easier to explode donors and faster (or slower) accretors post-RLOF.

From the black diamond onwards, we evolve the accretor as a single star with the same MESA setup until TAMS. The main-sequence track on which the accretor settles post-RLOF has a higher luminosity compared to the original track because of the accretion of mass, and it has also a slightly different slope due to the close-to-critical rotation and the accretion of matter partially processed in the core of the donor before mass transfer. The red point with errors in the bottom panel of Fig. 1 marks the approximate position of ζ Oph based on the analysis of Villamariz & Herrero (2005). The color of the track in Fig. 1 indicate that our accreting star spends about ~ 2 Myr within the represented errorbars after the end of RLOF. Assuming the kinematic age of 1.78 ± 0.21 (Neuhäuser et al. 2020), and estimating a remaining lifetime of the donor of ~ 0.5 Myr, this gives the correct timescale for the binary SN scenario.

We note that the observed position of ζ Oph on the HRD, and especially its relatively high T_{eff} would be hard to reproduce assuming initially less massive accretors (which would remain too cool even after accreting mass), or more equal initial mass ratio (which would produce a too evolved accretor at the onset of mass transfer).

Fig. 2 shows the rate of mass change for each star during RLOF. The top panel focuses on the donor star which loses mass to RLOF (cyan line) and wind mass loss (thin red line). The dashed blue lines show their combination resulting in the actual rate of mass change of the stars. The bottom panel shows instead the accreting star, which grows in mass because of the mass transfer. The entire duration of this case B stable RLOF (and thus of the feature in the bottom panel of Fig. 1 from the departure from the main-sequence to the black diamond) is only about 10^4 years. At peak the mass transfer rates reaches very high values above $10^{-2.5} M_\odot$ yr^{-1}, and taps into the optically thick matter of the donor.
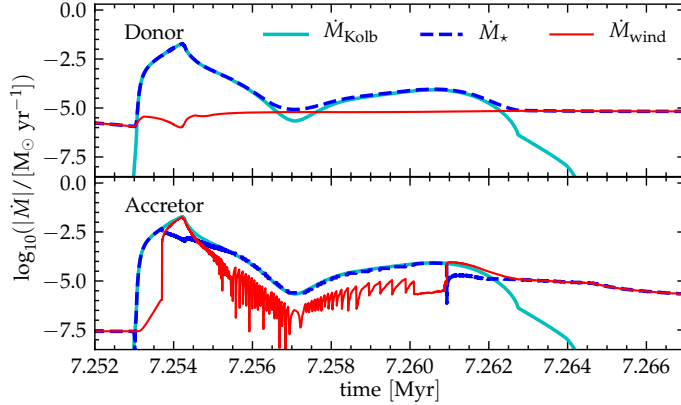
Figure 2. Mass transfer rates as a function of time during RLOF. The top (bottom) panel shows the donor (accretor) star. The cyan solid lines show the mass transfer rate between the two stars. The dashed blue lines show the actual change in the mass of the stars (due to the combination of wind, and accretion efficiency). The thin red lines show the wind mass loss rates. During RLOF the accretor reaches critical rotation, which leads to oscillations in the rotationally-enhahnced wind mass loss.

During RLOF, the total amount of mass lost by the donor is $\Delta M_{\mathrm{donor}} \simeq 10.6\,M_{\odot}$, of which only $\Delta M_{\mathrm{accretor}} \simeq 3.4\,M_{\odot}$ are successfully accreted. This corresponds to an overall mass transfer efficiency $\beta_{\mathrm{RLOF}} \equiv \Delta M_{\mathrm{accretor}}/\Delta M_{\mathrm{donor}} \simeq 0.3$, although the accretion efficiency is *not* constant throughout the mass transfer, instead it depends on the radial and rotational evolution of the accreting star.

At the end of RLOF, the donor star briefly expands again ($T_{\mathrm{eff}} \simeq 10^{4.1}\,\mathrm{K}$, $L \simeq 10^{5.5}\,L_{\odot}$). This is due to the partial recombination of the now He-rich outer layers, which causes a transient surface convection layer. This causes the second broad peak in the mass transfer rates centered at $7.261\,\mathrm{Myrs}$. We find this to be the culprit of difficulties in modeling massive binaries transferring mass in older MESA releases, because although only a very small amount of mass is involved, this would lead to large radial expansion much beyond the donor's Roche lobe, and cause numerical problems.

The wind mass loss (in red) controls the accretion efficiency and thus the difference between the actual rate of change in mass of the accretor (thick dashed blue) and the rate at which mass is being transferred. At peak, where the red and the cyan lines overlap, mass transfer becomes very non-conservative, but for most of the evolution the (rotationally enhanced) wind removes only a fraction of the accreted mass. The interplay between the stellar radius and rotation causes the oscillations visible in the bottom panel, whose amplitude is generally lower than the RLOF mass transfer rate.

3.1. *Internal mixing and surface composition of the accretor*

MESA treats mixing processes in the diffusion approximation (Paxton et al. 2011). To illustrate the dominant processes throughout the accretor's evolution, we show in Fig. 3 the diffusion coefficients as a function of mass coordinate at selected times. Each panel corresponds to one of the thin blue crosses in the bottom panel of Fig. 1, and the gray shaded areas mark mass that is accreted during RLOF. The last panel roughly represents the predicted internal structure of ζ Oph as observed today.

In Fig. 3, the thin red lines correspond to convection, with the initial convective core of $\sim 6\,M_{\odot}$ clearly visible in the first panel. In all models, a tiny sub-surface convective region is also visible in the outermost layers (see e.g., Cantiello et al. 2021). The thin blue lines mark mixing processes that are not related to rotation, nor are any of the other processes explicitly shown, which in these models effectively means overshooting. The extension of the convective diffusion coefficient above the core in all panels is the typical behavior for an exponentially decreasing overshooting. Purple and pink represent semiconvection and thermohaline mixing, respectively. Before mass transfer (left-most panel), only a small amount of sub-surface thermohaline mixing occurs, with a mass extent comparable or smaller to the sub-surface convective zone, and no semiconvection occurs. The thick cyan line corresponds to the total diffusion coefficient, obtained as the sum of the diffusion coefficients for each process modeled: where the cyan line is not overlapping with the others, rotational mixing (and more specifically Eddington-Sweet meridional circulation) is the dominant process.

During RLOF (second and third panel), the spin up due to accretion causes an increase in the rotational mixing (cyan line in the outer layers), and the accretion of nuclearly processed material progressively widens the thermohaline mixing region at the surface. Late during the mass transfer (third panel), thermohaline mixing dominates the outermost layers – except within the sub-surface convective zone, but throughout most of the envelope rotation does the lion's share of the mixing. Thermohaline mixing and Eddington-Sweet circulations together mix inwards and dilute the CNO-enriched material coming from the donor's surface.

At the same time, the increase in the accretor mass drives rejuvenation (e.g., Schneider et al. 2016). This can be seen as a growth of the convective core from $\sim 6\,M_{\odot}$ to almost $\sim 8\,M_{\odot}$, plus the corresponding growth of the overshooting region. This mixes inward H-rich material resulting in an elongation of the accretor's
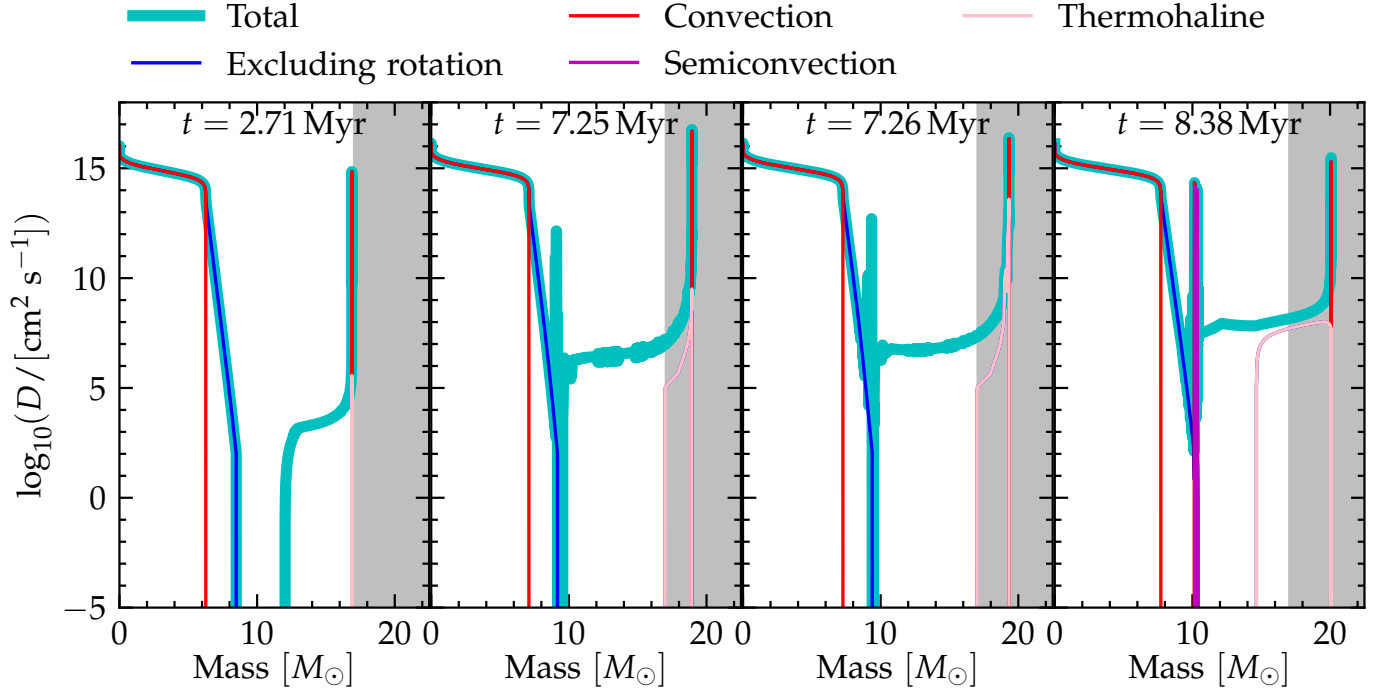
Figure 3. Mixing diffusion coefficients in the accretor star. From left to right, each panel shows times during the main sequence (t=2.71 Myr), right before the "v-shaped" feature during RLOF (t=7.25 Myr), close to the end of RLOF (t=7.26 Myr), and after mass transfer ($t = 8.38$ Myr). The total diffusion coefficient (thick cyan line) is obtained as the sum of non-rotational mixing processes (i.e., here overshooting, thin blue line), convection (shown in red), thermohaline mixing (pink) and semiconvection (in purple). The gray area corresponds to mass accreted during RLOF. The HRD position for each panel is marked by a thin blue cross in Fig. 1.

lifetime, and at the same time mixes outward CNO-equilibrium matter, connecting the N-rich core with the outer envelope polluted from the top.

Tab. 1 summarizes the surface properties of the accretor star at the time shown in the last panel of Fig. 3, that is shortly after the RLOF phase, while the model is still roughly at the observed position of ζ Oph.

Both the mass and radius agree reasonably well with the estimated from Villamariz & Herrero (2005) and previous work, i.e. $20\,M_\odot$ and $8.3 \pm 1.5\,R_\odot$, respectively. The surface rotational velocity in excess of $350\,\mathrm{km\,s^{-1}}$ is also in the correct ballpark albeit possibly on the low end. We discuss further rotation and angular momentum transport in Sec. 3.2. We report the surface H mass fraction[3], lower than primordial because of the accretion of nuclearly processed material, and the surface mass fraction of the most prominent species ^{4}He, ^{12}C, ^{14}N, ^{16}O. Assuming our surface H mass fraction X^1H, the corresponding mass fractions of ^{4}He, ^{12}C, ^{14}N, ^{16}O reported in Villamariz

& Herrero (2005) are $0.335195955^{+0.1372628808583865}_{-0.0549051523433546}$, $0.0005894097903485333 \pm 0.0004071498590763836$, $0.0020766539621156497 \pm 0.001434501736942355$, and $0.0053131989971199976 \pm 0.003670227842063826$. Our values are sensitive to the interplay between several poorly understood processes treated in one dimension: mass accretion efficiency, rotationally enhanced wind mass loss, thermohaline, and inward rotational mixing. Therefore, although not perfect, we consider the match with the mass fractions reported by Villamariz & Herrero (2005) surprisingly satisfactory. ■ [**fix numbers**] ■

We now turn to describe the difference between the mixing processes happening in a single rotating massive stars and in our accretor model. Fig. 4 shows the mass fraction of ^{14}N as a function of mass coordinate along the evolution of three $20\,M_\odot$ stars initialized with $\omega/\omega_{\mathrm{crit}} = 0.2, 0.3, 0.4, 0.5$ (computed with an otherwise identical setup as our binary model), and in the last panel our accretor model. The dotted red line marks the primordial mass fraction of ^{14}N for the adopted $Z = 0.01$, the thin dashed lines mark the surface value at TAMS. The colored tracks show selected

---

[3] This is needed to convert mass fractions reported here into $\varepsilon(X) = 12 + \log_{10}(N_X/N_H)$, where N_X and N_H are the number fractions of species X and H, respectively.

M [$M_\odot$]	R [$R_\odot$]	$\log_{10}(\omega/[\text{s}^{-1}])$	v_{rot} [km s^{-1}]	$X(^1\text{H})$	$X(^4\text{He})$	$X(^{12}\text{C})$	$X(^{14}\text{N})$	$X(^{16}\text{O})$
20.1	9.6	-4.263	366.1	0.678010	0.312093	0.001344	0.001340	0.004148

Table 1. Properties of the accretors shortly after the end of RLOF (last thin blue cross in Fig. 1)

profiles throughout the main sequence, with lighter colors corresponding to more evolved stars.
■ [define ω and ω_{crit} somewhere] ■
The solid red line, and red shaded area ■ [fix plot and numbers, they don't correspond!!] ■ across all panels show the ^{14}N from Villamariz & Herrero (2005) (assuming a surface hydrogen mass fraction of 0.7): the mass fraction of ^{14}N alone is not sufficient to distinguish with these models, and already a moderate $\omega/\omega_{\text{crit}} \geq 0.3$ is sufficient for models to reach the lower-limit of the error bar.
The typical evolution
■ [maybe table with surface mass fractions at the last profile?] ■

3.2. *Angular momentum transport and internal structure*

■ [discuss rotation rate and radius] ■

4. ROBUSTNESS OF THE MODEL

In this section we investigate the sensitivity of our results to physical parameters.
■ [How to present results? Table? Showing what? surface mass fractions, rotation, L, Teff] ■
■ [Binary parameters:

- M_1
- M_2
- P
- J-accretion

] ■
■ [Single star parameters:

- thermohaline mixing
- Eddington-Sweet circulations
- metallicity

] ■
■ [others?] ■

5. DISCUSSION

5.1. *Free parameters in the treatment of mass transfer*

We regulate the accretion efficiency through the rotational enhancement of mass loss (e.g. Langer 1998). ■ [maybe move β_{RLOF} here] ■. However, (??) argued that accretion of mass (but no angular momentum) might be possible even at critical rotation.

5.2. *The explosion of the former companion*

Throughout this study, we have assumed the "binary SN scenario": after the mass transfer phase, the explosion of the donor breaks the binary and ejects the accretor with roughly its pre-explosion velocity (e.g., Renzo et al. 2019). This is the fate of the majority of massive binary systems, and ζ Oph might be the best example of this scenario (e.g., Blaauw 1952, 1961; Hoogerwerf et al. 2000). Neuhäuser et al. (2020) suggested not only the companion successfully exploded, but that the explosion produced radioactive ^{60}Fe which polluted Earth. From kinematic and orbital considerations they estimated a natal kick of $\sim$250 km s^{-1}, which would be sufficiently large to unbind the binary.■ [check, be more precise] ■

However, we have so far neglected the impact of the explosion on the structure of the accretor star. The blast wave will hit the companion at a ■ [estimate solid angle] ■ causing mass loss – directly via ablation and by injecting energy in the envelope, inflating it and enhancing its wind (Wheeler et al. 1975; Tauris & Takens 1998; Podsiadlowski 2003; Hirai et al. 2018). ■ [estimate mass loss] ■
Because of the SN shock, the just ejected new runaway star might appear bloated and redder (long before it overtakes the slowing SN remnant). Hydrodynamical simulations of a non-rotating star with a SN shock suggest that within ■ [X] ■ the star returns in equilibrium Hirai et al. (2018). The impact of this brief out of thermal equilibrium phase on the stellar spin should be investigated further.
The SN ejecta might also pollute the surface of the runaway depositing processed nuclear material (e.g. Przybilla et al. 2008). However, enhahnced mass loss, and rapid rotating might rapidly dilute the yields. ■ [improve this sec.] ■

6. CONCLUSIONS

We have demonstrated that self-consistent one-dimensional calculations of coupled stellar models with masses $\gtrsim 20\,M_\odot$ are possible with the MESA software instrument. As a first application, we focused on find-
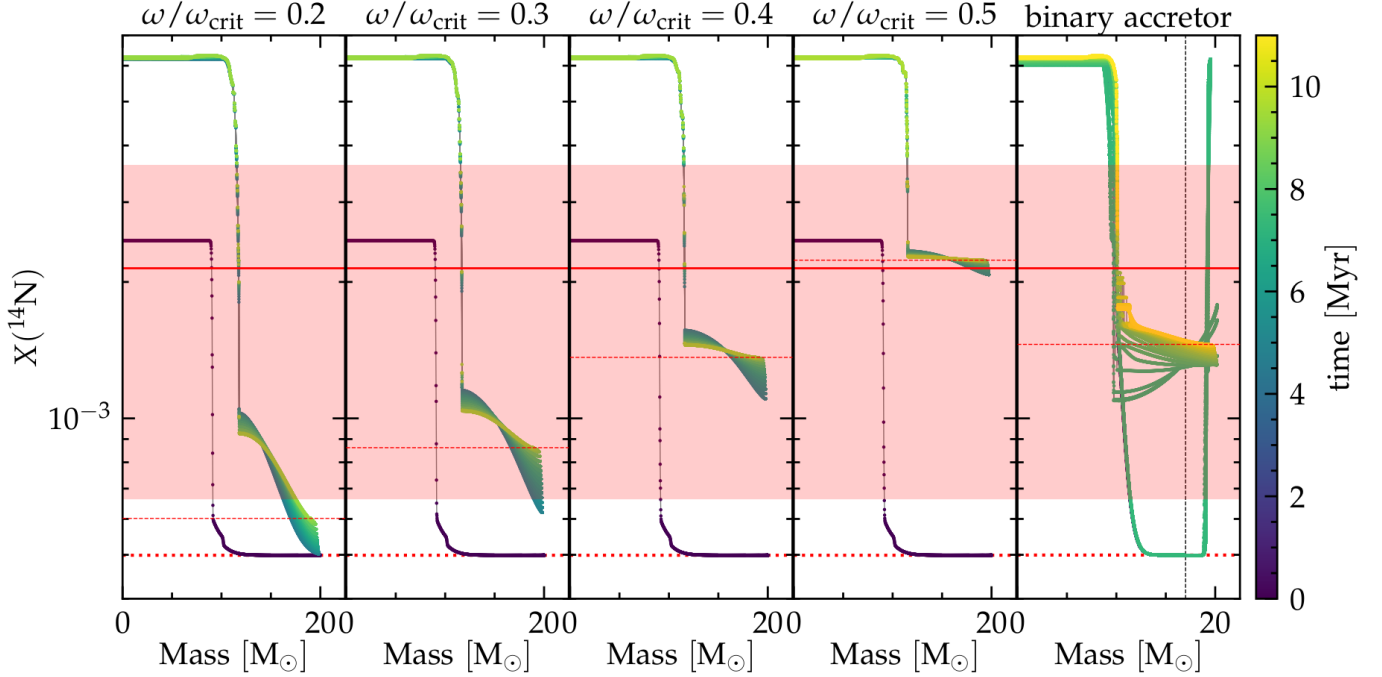
Figure 4. ^{14}N mass fraction as a function of mass coordinate for $20\,M_\odot$ single star models with increasing $\omega/\omega_{\rm crit}$ at birth (first four panels), and for the accretor of our fiducial binary. The dotted thick red line marks the primordial value, the thin dashed red line marks the surface value at TAMS. In the last panel, the thin vertical dashed line shows the initial total mass of the accretor. The colors of each profile go from dark to light at TAMS, and selected profiles along the main sequence are shown. The solid red line and the shaded region correspond to the mass fraction of ^{14}N estimated by Villamariz & Herrero (2005) assuming a surface H mass fraction of 0.7: the abundance of ^{14}N alone is not strongly constraining.
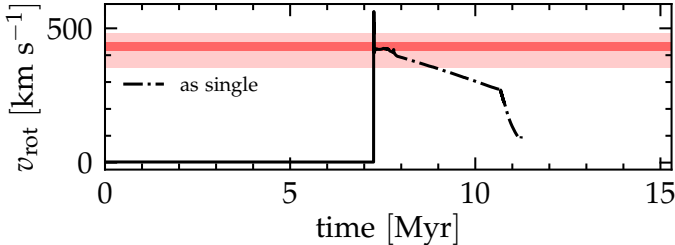
Figure 5. Surface averaged rotation rate for the accretor model. Shortly after $\sim 7\,$Myr the mass transfer quickly spins up the accretor at critical rotation. By the time the donor detaches from the RLOF the accretor is still spinning at $\sim 400\,{\rm km\,s^{-1}}$. At this point (beginning of the dot-dashed line), we continue the evolution as a single star, and the accretor quickly spins down. Note however that we use a wind mass-loss rate from Vink et al. (2001), which is observed to be ~ 2 orders of magnitude too high.

ing a model for ζ Oph, assuming its runaway nature is explained by the binary SN scenario.

We found that it is likely possible to explain its surface composition without assuming that the surface excess of

He and N comes from within the star. Instead, this material comes from the receding core of the donor star. Therefore, the present day abundances constrain the accretion efficiency and mixing in the accretor.

ζ Oph should therefore *not* be used to test models of rotational mixing in single star evolution, nor its more extreme version of chemically homogeneous evolution.

Software: mesaPlot (Farmer 2018), mesaSDK (Townsend 2018), ipython/jupyter (Pérez & Granger 2007), matplotlib (Hunter 2007), NumPy (van der Walt et al. 2011), MESA(Paxton et al. 2011, 2013, 2015, 2018, 2019)

APPENDIX

A. MESA SETUP

■ [MLT–?] ■

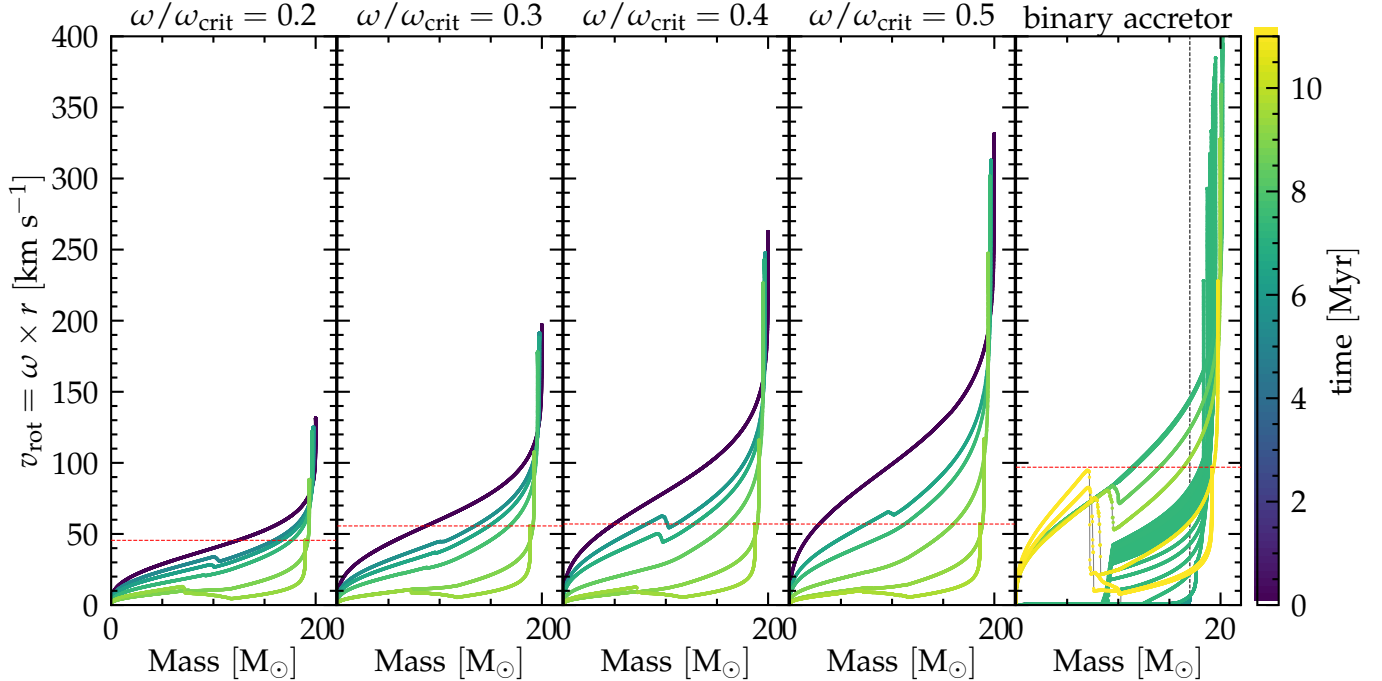■ [possibly move to methods] ■ We use MESA version 15140 to compute our models. The MESA

Figure 6. Internal rotational profile for $20\,M_\odot$ single star models with increasing $\omega/\omega_{\mathrm{crit}}$ at birth (first four panels), and for the accretor of our fiducial binary. As in Fig. 4, the colors go from dark (close to ZAMS) to light at TAMS, and the thin dashed red line mark the TAMS surface rotation rate. In the last panel, the thin vertical dashed line shows the initial total mass of the accretor. We note that at TAMS the core of the accretor is rotating almost as fast as its surface, and both are faster than the surface of single star models.

equation of state (EOS) is a blend of the OPAL Rogers & Nayfonov (2002), SCVH Saumon et al. (1995), PTEH Pols et al. (1995), HELM Timmes & Swesty (2000), and PC Potekhin & Chabrier (2010) EOSes. ■ [check if updated EOS?] ■

Radiative opacities are primarily from OPAL (Iglesias & Rogers 1993, 1996), with low-temperature data from Ferguson et al. (2005) and the high-temperature, Compton-scattering dominated regime by Buchler & Yueh (1976). Electron conduction opacities are from Cassisi et al. (2007).

Nuclear reaction rates are a combination of rates from NACRE (Angulo et al. 1999), JINA REACLIB (Cyburt et al. 2010), plus additional tabulated weak reaction rates Fuller et al. (1985); Oda et al. (1994); Langanke & Martínez-Pinedo (2000). Screening is included via the prescription of Chugunov et al. (2007). Thermal neutrino loss rates are from Itoh et al. (1996). We use a 22-isotope nuclear network (`approx_21_plus_cr56`).

The inlists, processing scripts, and model output will be made available at link.

B. RESOLUTION TESTS

B.1. *Spatial resolution*

REFERENCES

Almeida, L. A., Sana, H., Taylor, W., et al. 2017, A&A, 598, A84, doi: 10.1051/0004-6361/201629844

Angulo, C., Arnould, M., Rayet, M., et al. 1999, Nuclear Physics A, 656, 3, doi: 10.1016/S0375-9474(99)00030-5

Belczynski, K., Holz, D. E., Bulik, T., & O'Shaughnessy, R. 2016, Nature, 534, 512, doi: 10.1038/nature18322

Blaauw, A. 1952, BAN, 11, 414

—. 1961, BAN, 15, 265

Blaauw, A. 1993, in Astronomical Society of the Pacific Conference Series, Vol. 35, Massive Stars: Their Lives in the Interstellar Medium, ed. J. P. Cassinelli & E. B. Churchwell, 207

Blagorodnova, N., Klencki, J., Pejcha, O., et al. 2021, arXiv e-prints, arXiv:2102.05662. https://arxiv.org/abs/2102.05662

Bodensteiner, J., Baade, D., Greiner, J., & Langer, N. 2018, A&A, 618, A110, doi: 10.1051/0004-6361/201832722

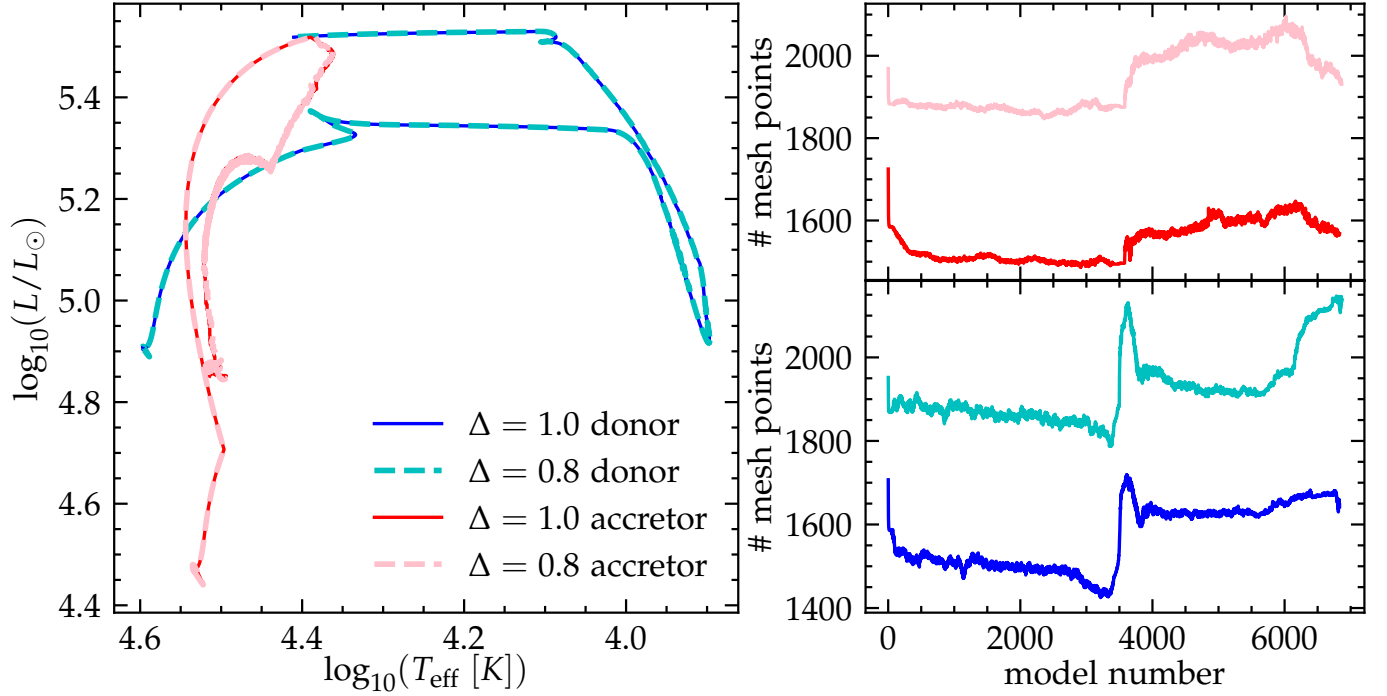Braun, H., & Langer, N. 1995, A&A, 297, 483

Figure 7. Left: HRD comparison for our fiducial binary model varying the number of mesh points. We only show the evolution until our definition of RLOF detachment. Right: number of mesh points as a function of timestep number. In both panels, the blue/cyan tracks show the donor stars, the red/pink tracks show the accretor. Thicker dashed lines correspond to the models at higher resolution (i.e., lower Δ which indicates the value of mesh_delta_coeff).

Broekgaarden, F. S., Berger, E., Neijssel, C. J., et al. 2021, arXiv e-prints, arXiv:2103.02608.
https://arxiv.org/abs/2103.02608

Brott, I., de Mink, S. E., Cantiello, M., et al. 2011, A&A, 530, A115, doi: 10.1051/0004-6361/201016113

Buchler, J. R., & Yueh, W. R. 1976, ApJ, 210, 440, doi: 10.1086/154847

Cantiello, M., Lecoanet, D., Jermyn, A. S., & Grassitelli, L. 2021, arXiv e-prints, arXiv:2102.05670.
https://arxiv.org/abs/2102.05670

Cantiello, M., Yoon, S., Langer, N., & Livio, M. 2007, A&A, 465, L29

Cassisi, S., Potekhin, A. Y., Pietrinferni, A., Catelan, M., & Salaris, M. 2007, ApJ, 661, 1094, doi: 10.1086/516819

Chugunov, A. I., Dewitt, H. E., & Yakovlev, D. G. 2007, PhRvD, 76, 025028, doi: 10.1103/PhysRevD.76.025028

Claret, A., & Torres, G. 2017, ApJ, 849, 18, doi: 10.3847/1538-4357/aa8770

Cyburt, R. H., Amthor, A. M., Ferguson, R., et al. 2010, ApJS, 189, 240, doi: 10.1088/0067-0049/189/1/240

De Donder, E., Vanbeveren, D., & van Bever, J. 1997, A&A, 318, 812

de Jager, C., Nieuwenhuijzen, H., & van der Hucht, K. A. 1988, A&AS, 72, 259

Eldridge, J. J., Langer, N., & Tout, C. A. 2011, MNRAS, 414, 3501, doi: 10.1111/j.1365-2966.2011.18650.x

Evans, F. A., Renzo, M., & Rossi, E. M. 2020, arXiv e-prints, arXiv:2006.00849.
https://arxiv.org/abs/2006.00849

Farmer, R. 2018, rjfarmer/mesaplot, doi: 10.5281/zenodo.1441329

Ferguson, J. W., Alexander, D. R., Allard, F., et al. 2005, ApJ, 623, 585, doi: 10.1086/428642

Fuller, G. M., Fowler, W. A., & Newman, M. J. 1985, ApJ, 293, 1, doi: 10.1086/163208

Götberg, Y., de Mink, S. E., & Groh, J. H. 2017.
https://arxiv.org/abs/1701.07439

Götberg, Y., de Mink, S. E., Groh, J. H., et al. 2018, A&A, 615, A78, doi: 10.1051/0004-6361/201732274

Heger, A., Langer, N., & Woosley, S. E. 2000, ApJ, 528, 368

Hellings, P. 1983, Ap&SS, 96, 37, doi: 10.1007/BF00661941

—. 1984, Ap&SS, 104, 83, doi: 10.1007/BF00653994

Herrero, A., Kudritzki, R. P., Vilchez, J. M., et al. 1992, A&A, 261, 209

Herwig, F. 2000, A&A, 360, 952

Hirai, R., Podsiadlowski, P., & Yamada, S. 2018.
https://arxiv.org/abs/1803.10808

Hoogerwerf, R., de Bruijne, J. H. J., & de Zeeuw, P. T. 2000, ApJL, 544, L133, doi: 10.1086/317315

—. 2001, A&A, 365, 49, doi: 10.1051/0004-6361:20000014

Hunter, J. D. 2007, Computing In Science & Engineering, 9, 90

Iglesias, C. A., & Rogers, F. J. 1993, ApJ, 412, 752, doi: 10.1086/172958

—. 1996, ApJ, 464, 943, doi: 10.1086/177381

Itoh, N., Hayashi, H., Nishikawa, A., & Kohyama, Y. 1996, ApJS, 102, 411, doi: 10.1086/192264

Kippenhahn, R., Ruschenplatt, G., & Thomas, H.-C. 1980, A&A, 91, 175

Kippenhahn, R., & Weigert, A. 1967, ZA, 65, 251

Klencki, J., Nelemans, G., Istrate, A. G., & Chruslinska, M. 2021, A&A, 645, A54, doi: 10.1051/0004-6361/202038707

Kolb, U., & Ritter, H. 1990, A&A, 236, 385

Langanke, K., & Martínez-Pinedo, G. 2000, Nuclear Physics A, 673, 481, doi: 10.1016/S0375-9474(00)00131-7

Langer, N. 1998, A&A, 329, 551

Langer, N., Fricke, K. J., & Sugimoto, D. 1983, A&A, 126, 207

Laplace, E., Götberg, Y., de Mink, S. E., Justham, S., & Farmer, R. 2020, A&A, 637, A6, doi: 10.1051/0004-6361/201937300

Laplace, E., Justham, S., Renzo, M., et al. 2021, arXiv e-prints, arXiv:2102.05036. https://arxiv.org/abs/2102.05036

Law-Smith, J. A. P., Everson, R. W., Ramirez-Ruiz, E., et al. 2020, arXiv e-prints, arXiv:2011.06630. https://arxiv.org/abs/2011.06630

Maeder, A., & Meynet, G. 2000, ARA&A, 38, 143, doi: 10.1146/annurev.astro.38.1.143

Marcolino, W. L. F., Bouret, J. C., Martins, F., et al. 2009, A&A, 498, 837, doi: 10.1051/0004-6361/200811289

Mason, B. D., Hartkopf, W. I., Gies, D. R., Henry, T. J., & Helsel, J. W. 2009, AJ, 137, 3358, doi: 10.1088/0004-6256/137/2/3358

Meynet, G., & Maeder, A. 2000, A&A, 361, 101

Murphy, S. J., Joyce, M., Bedding, T. R., White, T. R., & Kama, M. 2021, MNRAS, 502, 1633, doi: 10.1093/mnras/stab144

Neo, S., Miyaji, S., Nomoto, K., & Sugimoto, D. 1977, PASJ, 29, 249

Neuhäuser, R., Gießler, F., & Hambaryan, V. V. 2020, MNRAS, 498, 899, doi: 10.1093/mnras/stz2629

Oda, T., Hino, M., Muto, K., Takahara, M., & Sato, K. 1994, Atomic Data and Nuclear Data Tables, 56, 231, doi: 10.1006/adnd.1994.1007

Packet, W. 1981, A&A, 102, 17

Paxton, B., Bildsten, L., Dotter, A., et al. 2011, ApJS, 192, 3, doi: 10.1088/0067-0049/192/1/3

Paxton, B., Cantiello, M., Arras, P., et al. 2013, ApJS, 208, 4, doi: 10.1088/0067-0049/208/1/4

Paxton, B., Marchant, P., Schwab, J., et al. 2015, ApJS, 220, 15, doi: 10.1088/0067-0049/220/1/15

Paxton, B., Schwab, J., Bauer, E. B., et al. 2018, ApJS, 234, 34, doi: 10.3847/1538-4365/aaa5a8

Paxton, B., Smolec, R., Gautschy, A., et al. 2019. https://arxiv.org/abs/1903.01426

Pérez, F., & Granger, B. E. 2007, Computing in Science & Engineering, 9, 21

Perna, R., Duffell, P., Cantiello, M., & MacFadyen, A. I. 2014, ApJ, 781, 119, doi: 10.1088/0004-637X/781/2/119

Podsiadlowski, P. 2003, arXiv e-prints, astro. https://arxiv.org/abs/astro-ph/0303660

Pols, O. R., & Marinus, M. 1994, A&A, 288, 475

Pols, O. R., Tout, C. A., Eggleton, P. P., & Han, Z. 1995, MNRAS, 274, 964, doi: 10.1093/mnras/274.3.964

Potekhin, A. Y., & Chabrier, G. 2010, Contributions to Plasma Physics, 50, 82, doi: 10.1002/ctpp.201010017

Przybilla, N., Nieva, M. F., Heber, U., & Butler, K. 2008, The Astrophysical Journal, 684, L103, doi: 10.1086/592245

Renzo, M., Zapartas, E., de Mink, S. E., et al. 2019, A&A, 624, A66, doi: 10.1051/0004-6361/201833297

Rogers, F. J., & Nayfonov, A. 2002, ApJ, 576, 1064, doi: 10.1086/341894

Sana, H., de Mink, S. E., de Koter, A., et al. 2012, Science, 337, 444, doi: 10.1126/science.1223344

Saumon, D., Chabrier, G., & van Horn, H. M. 1995, ApJS, 99, 713, doi: 10.1086/192204

Schneider, F. R. N., Podsiadlowski, P., Langer, N., Castro, N., & Fossati, L. 2016, MNRAS, 457, 2355, doi: 10.1093/mnras/stw148

Schneider, F. R. N., Podsiadlowski, P., & Müller, B. 2021, A&A, 645, A5, doi: 10.1051/0004-6361/202039219

Sota, A., Maíz Apellániz, J., Morrell, N. I., et al. 2014, ApJS, 211, 10, doi: 10.1088/0067-0049/211/1/10

Spruit, H. C. 2002, A&A, 381, 923, doi: 10.1051/0004-6361:20011465

Sweet, P. A. 1950, MNRAS, 110, 548, doi: 10.1093/mnras/110.6.548

Tauris, T. M., & Takens, R. J. 1998, A&A, 330, 1047

Tauris, T. M., Kramer, M., Freire, P. C. C., et al. 2017, ApJ, 846, 170, doi: 10.3847/1538-4357/aa7e89

Tetzlaff, N., Neuhäuser, R., Hohle, M. M., & Maciejewski, G. 2010, MNRAS, 402, 2369, doi: 10.1111/j.1365-2966.2009.16093.x

Timmes, F. X., & Swesty, F. D. 2000, ApJS, 126, 501, doi: 10.1086/313304

12

Townsend, R. 2018, MESA SDK for Linux: 20180822, doi: 10.5281/zenodo.2603170

van der Walt, S., Colbert, S. C., & Varoquaux, G. 2011, Computing in Science Engineering, 13, 22, doi: 10.1109/MCSE.2011.37

van Rensbergen, W., Vanbeveren, D., & De Loore, C. 1996, A&A, 305, 825

Villamariz, M. R., & Herrero, A. 2005, A&A, 442, 263, doi: 10.1051/0004-6361:20052848

Vink, J. S., Davies, B., Harries, T. J., Oudmaijer, R. D., & Walborn, N. R. 2009, A&A, 505, 743, doi: 10.1051/0004-6361/200912610

Vink, J. S., de Koter, A., & Lamers, H. J. G. L. M. 2000, A&A, 362, 295

—. 2001, A&A, 369, 574, doi: 10.1051/0004-6361:20010127

Walker, G. A. H., Yang, S., & Fahlman, G. G. 1979, ApJ, 233, 199, doi: 10.1086/157381

Wang, C., Langer, N., Schootemeijer, A., et al. 2020, ApJL, 888, L12, doi: 10.3847/2041-8213/ab6171

Wheeler, J. C., Lecar, M., & McKee, C. F. 1975, ApJ, 200, 145, doi: 10.1086/153771

Yoon, S.-C., Langer, N., & Norman, C. 2006, A&A, 460, 199, doi: 10.1051/0004-6361:20065912

Zapartas, E., de Mink, S. E., Justham, S., et al. 2021, A&A, 645, A6, doi: 10.1051/0004-6361/202037744

—. 2019. https://arxiv.org/abs/1907.06687

Zehe, T., Mugrauer, M., Neuhäuser, R., et al. 2018, Astronomische Nachrichten, 339, 46, doi: 10.1002/asna.201713383